Research Article

Haar-Wavelet-Based Just Noticeable Distortion Model for Transparent Watermark

Lu-Ting Ko,[1] Jwu-E Chen,[1] Hsi-Chin Hsin,[2] Yaw-Shih Shieh,[3] and Tze-Yun Sung[3]

[1] *Department of Electrical Engineering, National Central University, Chungli City 320-01, Taiwan*
[2] *Department of Computer Science and Information Engineering, National United University, Miaoli 360-03, Taiwan*
[3] *Department of Electronics Engineering, Chung Hua University, Hsinchu City 300-12, Taiwan*

Correspondence should be addressed to Tze-Yun Sung, bobsung@chu.edu.tw

Watermark transparency is required mainly for copyright protection. Based on the characteristics of human visual system, the just noticeable distortion (JND) can be used to verify the transparency requirement. More specifically, any watermarks whose intensities are less than the JND values of an image can be added without degrading the visual quality. It takes extensive experimentations for an appropriate JND model. Motivated by the texture masking effect and the spatial masking effect, which are key factors of JND, Chou and Li (1995) proposed the well-known full-band JND model for the transparent watermark applications. In this paper, we propose a novel JND model based on discrete wavelet transform. Experimental results show that the performance of the proposed JND model is comparable to that of the full-band JND model. However, it has the advantage of saving a lot of computation time; the speed is about 6 times faster than that of the full-band JND model.

1. Introduction

Watermarking is a process that hides information into a host image for the purpose of copyright protection, integrity checking, or captioning [1–3]. In order to achieve the transparency of watermark, many commonly used techniques are based on the characteristics of human visual system (HVS) [1–13]. Jayant et al. [14, 15] introduced a key concept known as the just noticeable distortion (JND), against which insignificant errors are not perceptible by human eyes. The JND of an image is in general dependent on background luminance, contrast of luminance, and dominant spatial frequency. It takes extensive experimentations to obtain an appropriate JND model.

Perceptual redundancies refer to the details of an image that are not perceivable by human eyes and therefore can be discarded without affecting the visual quality. As noted, human visual perception is sensitive to the contrast of luminance rather than their individual values [16–18]. In addition, the visibility of stimuli can be reduced by nonuniformly quantizing the background luminance [18–20]. The above known as the texture masking effect and the spatial masking effect are key factors that affect the JND of an image. Chou and Li proposed an effective model called the full-band JND model for the transparent watermark applications [21].

Wavelet transform provides an efficient multiresolution representation with various desirable properties such as subband decompositions with orientation selectivity and joint space-spatial frequency localization. In wavelet domain, the higher detailed information of a signal is projected onto the shorter basis function with higher spatial resolution; the lower detailed information is projected onto the larger basis function with higher spectral resolution. This matches the characteristics of HVS. Many wavelet-transform-based algorithms were proposed for various applications [22–34].

In this paper, we propose a wavelet-transform-based JND model for the watermark applications. It has the advantage of saving a lot of computation time. The remainder of the paper proceeds as follows. In Section 2, the full-band JND model is reviewed briefly. In Section 3, the discrete-wavelet-transform- (DWT-) based JND model is proposed. The modified DWT-based JND model and its evaluation are presented in Section 4. Conclusion can be found in Section 5.

2. Review of the Full-Band Just Noticeable Distortion (JND) Model

The full-band JND model [21] makes use of the properties of the HVS to measure the perceptual redundancies of an image. It produces the JND file for image pixels as follows:

$$\text{JND}(i,j) = \max\{f_1(bg(i,j), mg(i,j)), f_2(bg(i,j))\}, \tag{2.1}$$

where

$$f_1(bg(i,j), mg(i,j)) = mg(i,j) \times [\alpha(bg(i,j))] + \beta(bg(i,j)), \tag{2.2}$$

$$f_2(bg(i,j)) = \begin{cases} 17 \times \left(1 - \left(\dfrac{bg(i,j)}{127}\right)^{1/2}\right) + 3 & \text{for } bg(i,j) \le 127, \\[3mm] \dfrac{3}{128} \times (bg(i,j) - 127) + 3 & \text{for } bg(i,j) > 127, \end{cases} \tag{2.3}$$

$$\alpha(bg(i,j)) = bg(i,j) \times 0.0001 + 0.115, \tag{2.4}$$

$$\beta(bg(i,j)) = \frac{1}{2} - bg(i,j) \times 0.01, \tag{2.5}$$

$$bg(i,j) = \frac{1}{32} \sum_{w=1}^{5} \sum_{z=1}^{5} p(i-3+w, \ j-3+z) \times B(w,z), \tag{2.6}$$

$$mg(i,j) = \max_{k=1,2,3,4} \{|\text{grad}_k(i,j)|\}, \tag{2.7}$$

$$\text{grad}_k(i,j) = \frac{1}{16} \sum_{w=1}^{5} \sum_{z=1}^{5} p(i-3+w, j-3+z) \times G_k(w,z), \tag{2.8}$$

where $f_1(i,j)$ and $f_2(i,j)$ are the texture mask and the spatial mask, respectively, as mentioned in Section 1, $bg(i,j)$ is the average background luminance obtained by using a low-pass filter, $B(w,z)$, is given in Figure 1, $mg(i,j)$ is the maximum gradient obtained by using a set of high-pass filters, $G_k(w,z)$, $k = 1,2,3,4$, are given in Figure 2, functions $\alpha(\circ)$ and $\beta(\circ)$ are dependent on the average background luminance, and $p(i,j)$ is the luminance value at pixel position (i,j).

3. Discrete-Wavelet-Transform-Based JND Model

In this section, we propose a novel JND model based on discrete wavelet transform. It has the advantage of reducing computational complexity significantly.

3.1. Discrete Wavelet Transform

Discrete wavelet transform (DWT) provides an efficient multiresolution analysis for signals, Specifically, any finite energy signal $f(x)$ can be written by

$$f(x) = \sum_{n} S_J(n)\phi_{Jn}(x) + \sum_{\ell \leq J} \sum_{n} D_\ell(n)\psi_{\ell n}(x), \tag{3.1}$$

where ℓ denotes the resolution index with larger values meaning coarser resolutions, n is the translation index, $\psi(x)$ is a mother wavelet, $\phi(x)$ is the corresponding scaling function, $\psi_{\ell n}(x) = 2^{-\ell/2}\psi(2^{-\ell}x - n)$, $\phi_{\ell n}(x) = 2^{-\ell/2}\phi(2^{-\ell}x - n)$, $S_J(n)$ is the scaling coefficient representing the approximation information of $f(x)$ at the coarsest resolution 2^J, and $D_\ell(n)$ is the wavelet coefficient representing the detail information of $f(x)$ at resolution 2^ℓ. Coefficients $S_\ell(n)$ and $D_\ell(n)$ can be obtained from the scaling coefficient $S_{\ell-1}(n)$ at the next finer resolution $2^{\ell-1}$ by using 1-level DWT, which is given by

$$S_\ell(n) = \sum_{k} S_{\ell-1}(k)h(2n-k),$$

$$D_\ell(n) = \sum_{k} S_{\ell-1}(k)g(2n-k), \tag{3.2}$$

where $h(n) = \langle \phi, \phi_{-1,-n} \rangle$, $g(n) = \langle \psi, \phi_{-1,-n} \rangle$, and $\langle \cdot, \cdot \rangle$ denotes the inner product. It is noted that $h(n)$ and $g(n)$ are the corresponding low-pass filter and high-pass filter, respectively. Moreover, $S_{\ell-1}(n)$ can be reconstructed from $S_\ell(n)$ and $D_\ell(n)$ by using the inverse DWT, which is given by

$$S_{\ell-1}(n) = \sum_{k} S_\ell(k)\tilde{h}(n-2k) + \sum_{k} D_\ell(k)\tilde{g}(n-2k), \tag{3.3}$$

1	1	1	1	1
1	2	2	2	1
1	2	0	2	1
1	2	2	2	1
1	1	1	1	1

B

Figure 1: Low-pass filter used in (2.6).

where $\tilde{h}(n) = h(-n)$ and $\tilde{g}(n) = g(-n)$.

For image applications, 2D DWT can be obtained by using the tensor product of 1D DWT. Among wavelets, Haar wavelet [22] is the simplest one, which has been widely used for many applications. The low-pass filter and high-pass filter of Haar wavelet are as follows:

$$h(0) = 0.5, \qquad h(1) = 0.5,$$
$$g(0) = 0.5, \qquad g(1) = -0.5. \tag{3.4}$$

Figures 3 and 4 show the row decomposition and the column decomposition using Haar wavelet, respectively. Notice that the column decomposition may follow the row decomposition, or vice versa, in 2D DWT:

$$LL = \frac{A + B + C + D}{4},$$
$$LH = \frac{A + B - C - D}{4},$$
$$HL = \frac{A - B + C - D}{4}, \tag{3.5}$$
$$HH = \frac{A - B - C + D}{4},$$

where A, B, C, and D are pixel values, and LL, LH, HL, and HH denote the approximation, detail information in the horizontal, vertical, and diagonal orientations, respectively, of the input image. Figure 5 shows 1-level, 2D DWT using Haar wavelet.

The LL subband of an image can be further decomposed into four subbands: $LLLL$, $LLLH$, $LLHL$, and $LLHH$ at the next coarser resolution, which together with LH, HL, and HH forms the 2-level DWT of the input image. Thus, higher level DWT can be obtained by decomposing the approximation subband in the recursive manner.
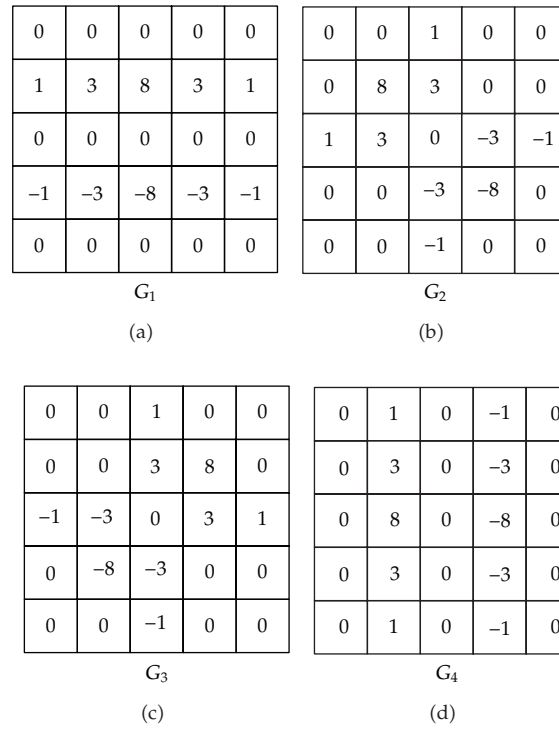
0	0	0	0	0
1	3	8	3	1
0	0	0	0	0
−1	−3	−8	−3	−1
0	0	0	0	0

G_1

(a)

0	0	1	0	0
0	8	3	0	0
1	3	0	−3	−1
0	0	−3	−8	0
0	0	−1	0	0

G_2

(b)

0	0	1	0	0
0	0	3	8	0
−1	−3	0	3	1
0	−8	−3	0	0
0	0	−1	0	0

G_3

(c)

0	1	0	−1	0
0	3	0	−3	0
0	8	0	−8	0
0	3	0	−3	0
0	1	0	−1	0

G_4

(d)

Figure 2: A set of high-pass filters used in (2.8).

A	B	C	D

Row decomposition →

$\dfrac{A+B}{2}$	$\dfrac{A-B}{2}$	$\dfrac{C+D}{2}$	$\dfrac{C-D}{2}$
L		H	
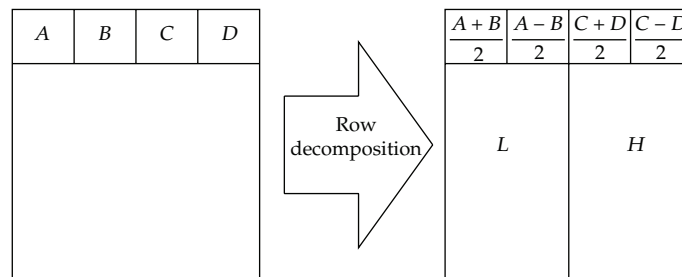
Figure 3: The row decomposition using Haar wavelet (A, B, C and D, are pixel values).

E		G	
F		H	
L		H	

Column decomposition →

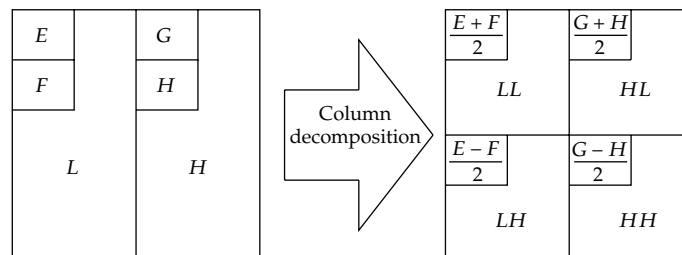| $\dfrac{E+F}{2}$		$\dfrac{G+H}{2}$	
LL		HL	
$\dfrac{E-F}{2}$		$\dfrac{G-H}{2}$	
LH		HH	

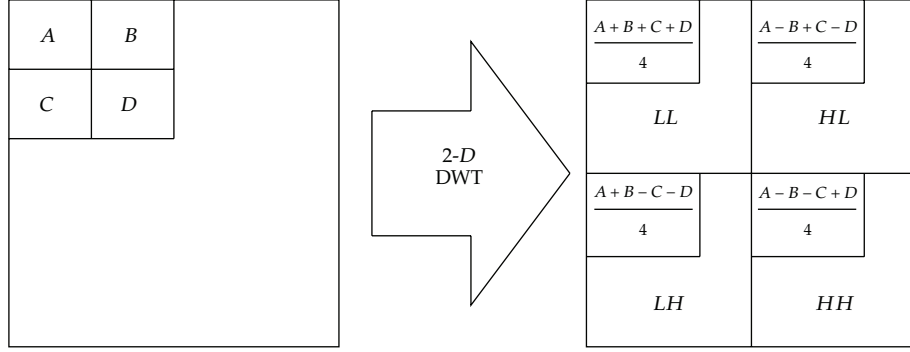**Figure 4:** The column decomposition using Haar wavelet (E, F, G, and H are pixel values).

Figure 5: 1-level 2D DWT using Haar wavelet (A, B, C, and D are pixel values).

3.2. Proposed DWT-Based JND Model

As mentioned in Section 2, the full-band JND model [21] consists of (2.1)–(2.8), which is essentially computation consuming. In order to simplify computational complexity, a novel JND model based on Haar wavelet is proposed as follows.

$$\text{JND}_{\text{DWT}}(i,j) = \max\{f_{1,\text{DWT}}(i,j), f_{2,\text{DWT}}(i,j)\}, \tag{3.6}$$

where $f_{1,\text{DWT}}(i,j)$ and $f_{2,\text{DWT}}(i,j)$ are the proposed texture mask and spatial mask, respectively, based on DWT, which are given by

$$f_{1,\text{DWT}}(i,j) = \left| D_i(i,j) \cdot \alpha\left[LLLL'(i,j)\right] + \beta\left[LLLL'(i,j)\right] \right|, \tag{3.7}$$

$$f_{2,\text{DWT}}(i,j) = \begin{cases} 17 \times \left(1 - \left[\dfrac{LLLL'(i,j)}{127}\right]^{1/2}\right) + 3 & \text{for } LLLL'(i,j) \leq 127, \\[4mm] \dfrac{3}{128} \times \left[LLLL'(i,j) - 127\right] + 3 & \text{for } LLLL'(i,j) > 127, \end{cases} \tag{3.8}$$

where

$$\alpha\left[LLLL'(i,j)\right] = LLLL'(i,j) \times 0.0001 + 0.115, \tag{3.9}$$

$$\beta\left[LLLL'(i,j)\right] = \frac{1}{2} - LLLL'(i,j) \times 0.01, \tag{3.10}$$

$$LLLL' = \mathbf{T_2 T_1}[LLLL]\mathbf{T_1^T T_2^T}, \tag{3.11}$$

$$\mathbf{T}_1 = \begin{bmatrix} 1 & 0 \\ 1 & 0 \\ 0 & 1 \\ 0 & 1 \end{bmatrix}_{4\times2}, \tag{3.12}$$

$$\mathbf{T}_2 = \begin{bmatrix} 1 & 0 & 0 & 0 \\ 1 & 0 & 0 & 0 \\ 0 & 1 & 0 & 0 \\ 0 & 1 & 0 & 0 \\ 0 & 0 & 1 & 0 \\ 0 & 0 & 1 & 0 \\ 0 & 0 & 0 & 1 \\ 0 & 0 & 0 & 1 \end{bmatrix}_{8\times4}. \tag{3.13}$$

$LLLL'$ is the modified $LLLL$, which replaces the low-pass filter $B(w, z)$ of the full-band JND model. $D_i(i, j)$ replaces the maximum gradient, $mg(i, j)$, which is given by

$$D_i(i, j) = \max\{|LH'(i, j)|, |HL'(i, j)|, |SL'_R(i, j)|, |SL'_L(i, j)|\}, \tag{3.14}$$

where

$$LH' = \mathbf{T_2}[LH]\mathbf{T_2^T}, \tag{3.15}$$

$$HL' = \mathbf{T_2}[HL]\mathbf{T_2^T}, \tag{3.16}$$

$$SL'_R = \mathbf{T_2}[SL_R]\mathbf{T_2^T}, \tag{3.17}$$

$$SL'_L = \mathbf{T_2}[SL_L]\mathbf{T_2^T}, \tag{3.18}$$

$$SL_R = \frac{LH + HL}{2}, \tag{3.19}$$

$$SL_L = \frac{LH - HL}{2}. \tag{3.20}$$

LH', HL', SL'_R, and SL'_L replace $G_1(w, z)$, $G_2(w, z)$, $G_3(w, z)$, and $G_4(w, z)$, respectively.

4. Modification of the DWT-Based JND Model

In this section, we introduce an adjustable parameter to modify the DWT-based JND model such that the computation time can be reduced significantly while the performance is comparable to that of the benchmark full-band JND model. The test images, namely, Lena, Cameraman, Baboon, Board, and Peppers are shown in the first row of Figure 12.
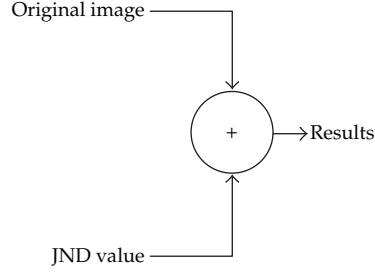
Figure 6: Distortion-tolerant evaluation model for the proposed JND model.

Table 1: PSNR comparisons of the benchmark full-band JND model, the proposed DWT-based JND model, and the modified DWT-based JND model.

JND model	Lena	Cameraman	Baboon	Board	Peppers
Full-band JND	32.7041	29.9122	34.0845	25.3486	30.3052
DWT-based JND	34.3301	31.7556	35.8156	30.8003	32.1375
The modified DWT-based JND	33.7117	30.9614	34.0931	25.7192	31.7148

4.1. Evaluation of JND Models

Figure 6 shows the distortion-tolerant model, which can be used to evaluate JND models. It takes the JND value as noise, adds to the original image, and computes the peak-signal-to-noise ratio (PSNR) defined as

$$\text{PSNR} = 20 \log\left(\frac{255}{\sqrt{\text{MSE}}}\right), \tag{4.1}$$

where MSE is the mean squared error, which is defined as

$$\text{MSE} = \frac{1}{m \times n} \sum_{i=0}^{m-1} \sum_{j=0}^{n-1} \left[\text{JND}(i,j)\right]^2, \tag{4.2}$$

where image size is $m \times n$. As shown in Table 1, the proposed DWT-based JND model is somewhat different from the benchmark full-band JND model in terms of the PSNR values.

4.2. Modified DWT-Based JND Model

Based on (2.1)–(2.3) and (3.6)–(3.8), one can examine the influences of the dominant mask, texture mask, and spatial mask for the full-band JND model and the DWT-based JND model, respectively. Their respective MSE values are shown in Table 2. As one can see, the proposed texture mask for the DWT-based JND model is less significant than that of the full-band JND model. Thus, we propose an adjustable parameter, K, to modify (3.17) and (3.18) as follows:

$$SL_R'' = K \cdot SL_R',$$
$$SL_L'' = K \cdot SL_L', \tag{4.3}$$
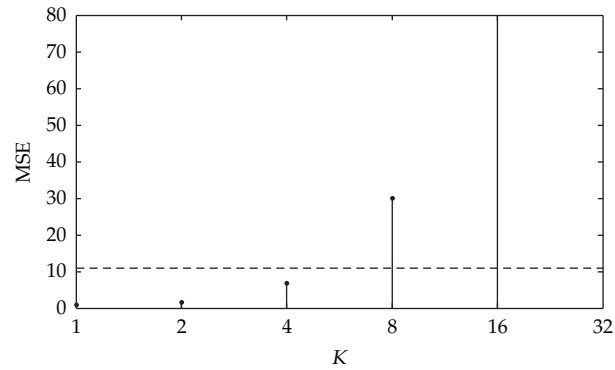
Figure 7: MSE values obtained by modifying the DWT-based texture mask using (4.3) with various K for Lena image; dashed line: MSE value obtained by using the texture mask of the full-band JND model.
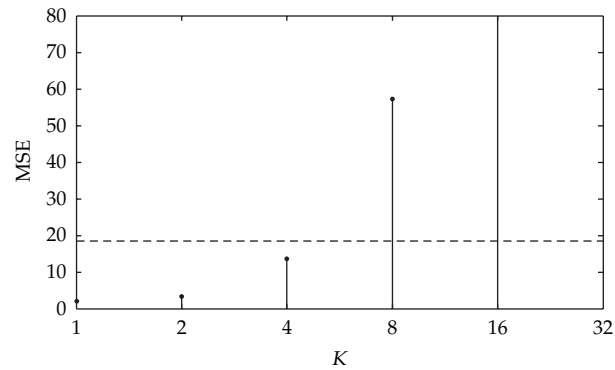
Figure 8: MSE values obtained by modifying the DWT-based texture mask using (4.3) with various K for Cameraman image; dashed line: MSE value obtained by using the texture mask of the full-band JND model.
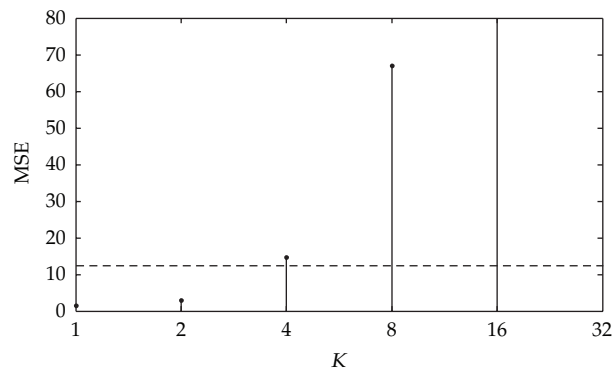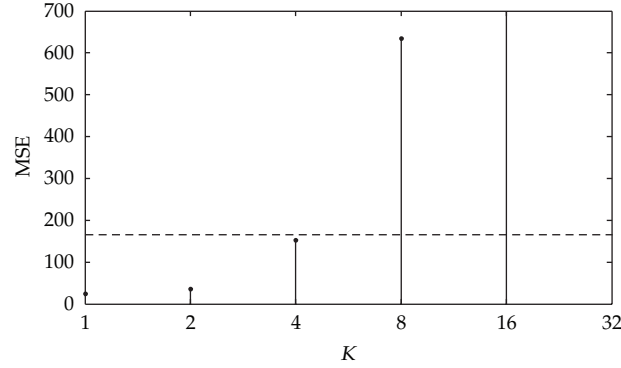

Figure 9: MSE values obtained by modifying the DWT-based texture mask using (4.3) with various K for Baboon image; dashed line: MSE value obtained by using the texture mask of the full-band JND model.

Figure 10: MSE values obtained by modifying the DWT-based texture mask using (4.3) with various K for Board image; dashed line: MSE value obtained by using the texture mask of the full-band JND model.

Figure 11: MSE values obtained by modifying the DWT-based texture mask using (4.3) with various K for Peppers image; dashed line: MSE value obtained by using the texture mask of the full-band JND model.
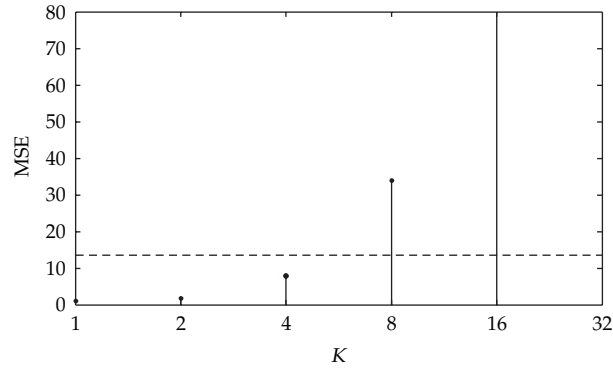
where SL_R'' and SL_L'' replace SL_R' and SL_L', respectively. Figures 7, 8, 9, 10, and 11 show the MSE values obtained by modifying the DWT-based texture mask with various K in (4.3). In this paper, the adjustable parameter K is set to 4 after extensive simulations. The performance of the modified DWT-based JND model with $K = 4$ is comparable to that of the full-band JND model in terms of the PSNR and MSE values as shown in Tables 1 and 2, respectively.

Figure 12 shows the noisy images obtained by adding the JND values to the original images (Figure 12(a)) using the full-band JND model (Figure 12(b)), the DWT-based JND model (Figure 12(c)), and the modified DWT-based JND model (Figure 12(d)). It is noted that the images in the second and fourth rows are almost indistinguishable from the original images. As a result, the modified DWT-based JND model is visually comparable to the full-band JND model.

### 4.3. Computation Complexity of the Proposed JND Models

In the full-band JND model, the computation of $bg(i, j)$ requires 9 multiplications per pixel, the computation of $mg(i, j)$ requires 28 multiplications per pixel, and the computation required for (2.2)–(2.5) is 6 multiplications per pixel. Thus, for an $n \times n$ image, it requires

(a)

(b)

(c)

(d)
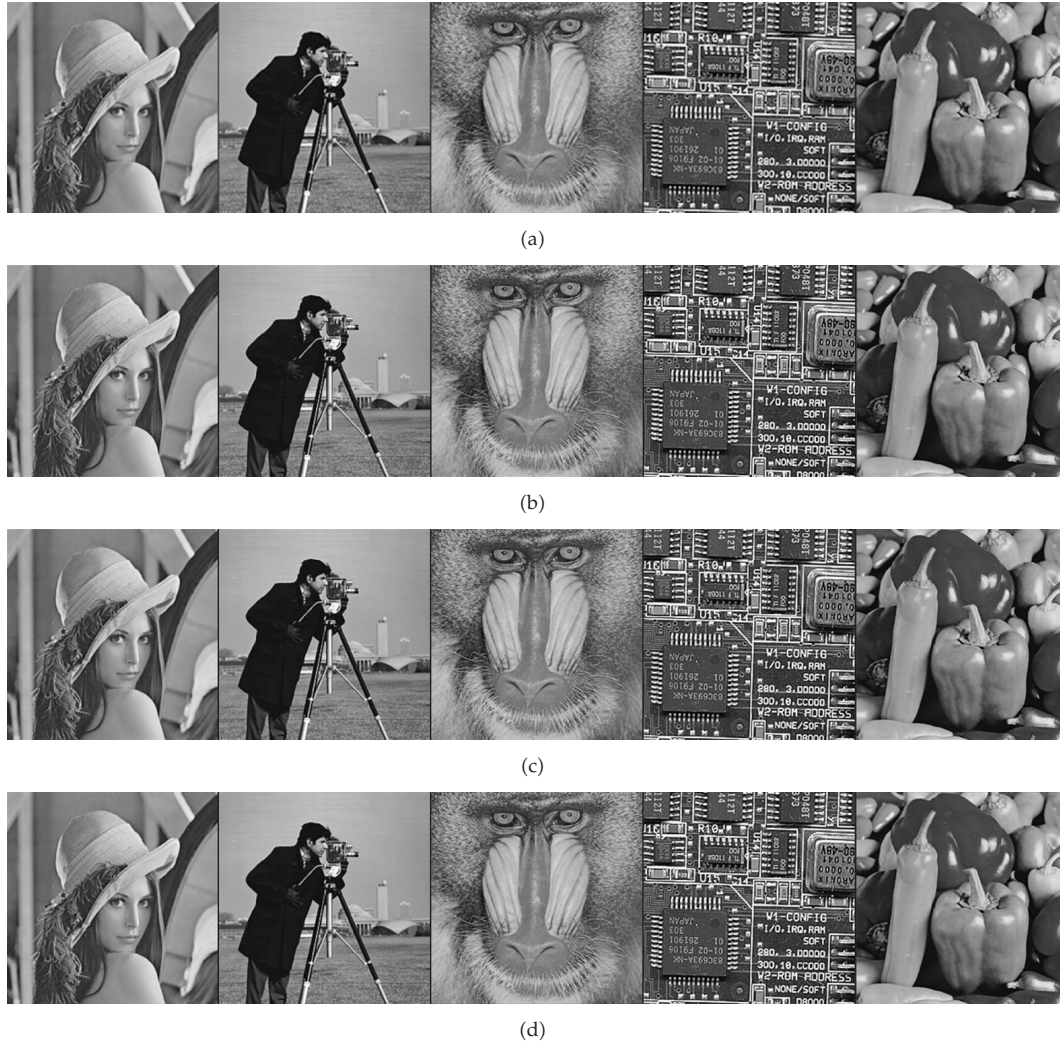
Figure 12: (a) The original images, namely, Lena, Cameraman, Baboon, Board, and Peppers; (b), (c), and (d) the noisy images obtained by adding the full-band JND values, the DWT-based JND values, and the modified DWT-based JND values, respectively.

Table 2: The MSE values due to the dominant mask (case 1), the spatial mask (case 2), and the texture mask (case 3) using the full-band JND model, the DWT-based JND model, and the modified DWT-based JND model.

JND model	Case	Lena	Cameraman	Baboon	Board	Peppers
	1	34.8876	66.3534	25.3878	189.7653	60.6121
Full-band JND	2	28.5202	53.0297	19.6219	41.7222	52.5825
	3	10.9574	18.4772	12.373	165.6492	12.583
	1	23.9924	43.4027	17.0419	54.0822	39.7492
DWT-based JND	2	23.9269	43.0406	16.942	38.4702	39.642
	3	0.972	2.1076	1.4603	24.4885	1.1393
	1	27.6254	52.1122	25.3378	174.244	43.8131
The modified DWT-based JND	2	23.9269	43.0406	16.942	38.4702	39.642
	3	6.9379	13.7233	14.7008	153.4052	7.8595
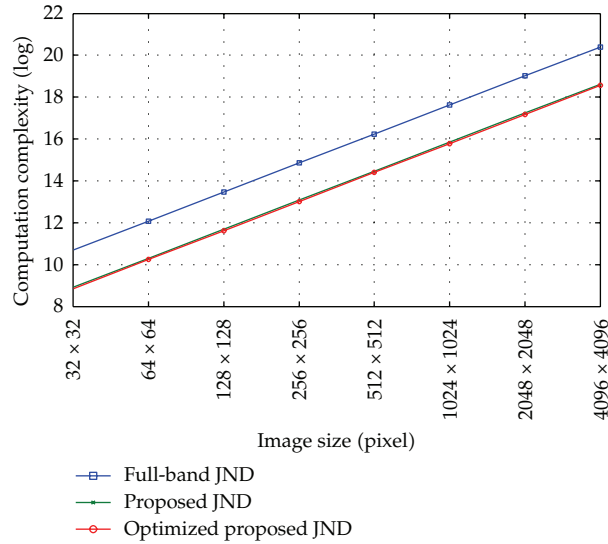
Figure 13: Log plot of numbers of multiplications required for the three JND models versus different image sizes.

$43n^2$ multiplications. In the proposed DWT-based JND model, the computations of LH', HL', $LLLL'$, SL'_R, and SL'_L require $(1/4)n^2$, $(1/4)n^2$, $(5/16)n^2$, $(1/4)n^2$, and $(1/4)n^2$ multiplications, respectively, for an $n \times n$ image, and the computation required for (3.7)–(3.10) is also 6 multiplications per pixel. Thus, for an $n \times n$ image, it requires $7.3125n^2$ multiplications. In the modified DWT-based JND model, as the computations of SL''_R and SL''_L require no multiplication, it only needs $6.8125n^2$ multiplications for an $n \times n$ image. Figure 13 shows the log plot of numbers of multiplications required for the three JND models versus different image sizes. As a result, the speed of the DWT-based JND model is about 6 times faster than that of the full-band JND model, which is the main advantage.

5. Conclusion

In this paper, an efficient DWT-based JND model is presented. It has the advantage of saving a lot of computation time while the performance is comparable to the benchmark full-band JND model. More specifically, the computation complexity of the proposed DWT-based JND model is only one sixth of that of the full-band JND model. As a result, it is suitable for the real-time applications.

Acknowledgment

References

[1] I. J. Cox, J. Kilian, F. T. Leighton, and T. Shamoon, "Secure spread spectrum watermarking for multimedia," *IEEE Transactions on Image Processing*, vol. 6, no. 12, pp. 1673–1687, 1997.

[2] M. D. Swanson, M. Kobayashi, and A. H. Tewfik, "Multimedia data-embedding and watermarking technologies," *Proceedings of the IEEE*, vol. 86, no. 6, pp. 1064–1087, 1998.

[3] M. Barni, F. Bartolini, and A. Piva, "Improved wavelet-based watermarking through pixel-wise masking," *IEEE Transactions on Image Processing*, vol. 10, no. 5, pp. 783–791, 2001.

[4] M. Kutter and S. Winkler, "A vision-based masking model for spread-spectrum image watermarking," *IEEE Transactions on Image Processing*, vol. 11, no. 1, pp. 16–25, 2002.

[5] C. De Vleeschouwer, J. F. Delaigle, and B. Macq, "Invisibility and application functionalities in perceptual watermarking - An overview," *Proceedings of the IEEE*, vol. 90, no. 1, pp. 64–77, 2002.

[6] Q. Li, C. Yuan, and Y. Z. Zhong, "Adaptive DWT-SVD domain image watermarking using human visual model," in *Proceedings of the 9th International Conference on Advanced Communication Technology (ICACT '07)*, pp. 1947–1951, February 2007.

[7] F. Autrusseau and P. L. Callet, "A robust image watermarking technique based on quantization noise visibility thresholds," *Signal Processing*, vol. 87, no. 6, pp. 1363–1383, 2007.

[8] H. S. Moon, T. You, M. H. Sohn, H. S. Kim, and D. S. Jang, "Expert system for low frequency adaptive image watermarking: using psychological experiments on human image perception," *Expert Systems with Applications*, vol. 32, no. 2, pp. 674–686, 2007.

[9] H. Qi, D. Zheng, and J. Zhao, "Human visual system based adaptive digital image watermarking," *Signal Processing*, vol. 88, no. 1, pp. 174–188, 2008.

[10] A. Koz and A. A. Alatan, "Oblivious spatio-temporal watermarking of digital video by exploiting the human visual system," *IEEE Transactions on Circuits and Systems for Video Technology*, vol. 18, no. 3, pp. 326–337, 2008.

[11] S. Y. Chen, Y. F. Li, and J. Zhang, "Vision processing for realtime 3-D data acquisition based on coded structured light," *IEEE Transactions on Image Processing*, vol. 17, no. 2, pp. 167–176, 2008.

[12] S. Y. Chen, H. Tong, Z. Wang, S. Liu, M. Li, and B. Zhang, "Improved generalized belief propagation for vision processing," *Mathematical Problems in Engineering*, vol. 2011, Article ID 416963, 12 pages, 2011.

[13] S. Y. Chen and Q. Guan, "Parametric shape representation by a deformable NURBS model for cardiac functional measurements," *IEEE Transactions on Biomedical Engineering*, vol. 58, no. 3, pp. 480–487, 2011.

[14] N. Jayant, "Signal compression: technology targets and research directions," *IEEE Journal on Selected Areas in Communications*, vol. 10, pp. 314–323, 1992.

[15] N. Jayant, J. Johnston, and R. Safranek, "Signal compression based on models of human perception," *Proceedings of the IEEE*, vol. 81, no. 10, pp. 1385–1422, 1993.

[16] R. F. Boyer and R. S. Spencer, "Thermal expansion and second-order transition effects in high polymers: part II. Theory," *Journal of Applied Physics*, vol. 16, no. 10, pp. 594–607, 1945.

[17] A. K. Jain, *Fundamentals of Digital Image Processing*, Prentice-Hall, Englewood Cliffs, NJ, USA, 1989.

[18] X. Yang, W. Lin, Z. Lu, E. Ong, and S. Yao, "Motion-compensated residue preprocessing in video coding based on just-noticeable-distortion profile," *IEEE Transactions on Circuits and Systems for Video Technology*, vol. 15, no. 6, pp. 742–751, 2005.

[19] J. Pandel, "Variable bit-rate image sequence coding with adaptive quantization," *Signal Processing*, vol. 3, no. 2-3, pp. 123–128, 1991.

[20] B. Girod, "Psychovisual aspects of image communication," *Signal Processing*, vol. 28, no. 3, pp. 239–251, 1992.

[21] C. H. Chou and Y. C. Li, "Perceptually tuned subband image coder based on the measure of just-noticeable-distortion profile," *IEEE Transactions on Circuits and Systems for Video Technology*, vol. 5, no. 6, pp. 467–476, 1995.

[22] B. S. Kim, I. J. Shim, M. T. Lim, and Y. J. Kim, "Combined preorder and postorder traversal algorithm for the analysis of singular systems by Haar wavelets," *Mathematical Problems in Engineering*, vol. 2008, Article ID 323080, 16 pages, 2008.

[23] G. Mattioli, M. Scalia, and C. Cattani, "Analysis of large-amplitude pulses in short time intervals: application to neuron interactions," *Mathematical Problems in Engineering*, vol. 2010, Article ID 895785, 15 pages, 2010.

[24] C. Cattani, "Harmonic wavelet approximation of random, fractal and high frequency signals," *Telecommunication Systems*, vol. 43, no. 3-4, pp. 207–217, 2010.

[25] C. Cattani, "Shannon wavelets theory," *Mathematical Problems in Engineering*, vol. 2008, Article ID 164808, 24 pages, 2008.

[26] A. Kudreyko and C. Cattani, "Application of periodized harmonic wavelets towards solution of eigenvalue problems for integral equations," *Mathematical Problems in Engineering*, vol. 2010, Article ID 570136, 8 pages, 2010.

[27] M. Li and W. Zhao, "Representation of a stochastic traffic bound," *IEEE Transactions on Parallel and Distributed Systems*, vol. 21, no. 9, Article ID 5342414, pp. 1368–1372, 2010.

[28] M. Li, "Generation of teletraffic of generalized Cauchy type," *Physica Scripta*, vol. 81, no. 2, Article ID 025007, 2010.

[29] M. Li, "Fractal time series-a tutorial review," *Mathematical Problems in Engineering*, vol. 2010, Article ID 157264, 26 pages, 2010.

[30] E. G. Bakhoum and C. Toma, "Specific mathematical aspects of dynamics generated by coherence functions," *Mathematical Problems in Engineering*, vol. 2011, Article ID 436198, 10 pages, 2011.

[31] E. G. Bakhoum and C. Toma, "Dynamical aspects of macroscopic and quantum transitions due to coherence function and time series events," *Mathematical Problems in Engineering*, vol. 2010, Article ID 428903, 13 pages, 2010.

[32] E. G. Bakhoum and C. Toma, "Mathematical transform of traveling-wave equations and phase aspects of quantum interaction," *Mathematical Problems in Engineering*, vol. 2010, Article ID /695208, 15 pages, 2010.

[33] T. Y. Sung and H. C. Hsin, "A hybrid image coder based on SPIHT algorithm with embedded block coding," *IEICE Transactions on Fundamentals of Electronics, Communications and Computer Sciences*, vol. E90-A, no. 12, pp. 2979–2984, 2007.

[34] H. C. Hsin and T. Y. Sung, "Adaptive selection and rearrangement of wavelet packets for quad-tree image coding," *IEICE Transactions on Fundamentals of Electronics, Communications and Computer Sciences*, vol. E91-A, no. 9, pp. 2655–2662, 2008.

Submit your manuscripts at
http://www.hindawi.com

Advances in
Operations Research

Advances in
Decision Sciences

Mathematical Problems
in Engineering

Algebra

Journal of
Probability and Statistics

The Scientific
World Journal

International Journal of
Differential Equations

International Journal of
Combinatorics

Advances in
Mathematical Physics

Journal of
Complex Analysis

Journal of
Mathematics

International Journal of
Stochastic Analysis

Abstract and
Applied Analysis

Discrete Dynamics in
Nature and Society

International
Journal of
Mathematics and
Mathematical
Sciences

Journal of
Discrete Mathematics

Journal of
Function Spaces

Journal of
Applied Mathematics

Journal of
Optimization